

# Quasiparticle spectra of Abrikosov vortices in a uniform supercurrent flow

C. Berthod

DPMC, University of Geneva, 24 quai Ernest-Ansermet, 1211 Geneva 4, Switzerland

(Dated: September 15, 2013)

We calculate the local density of states of a vortex in a two-dimensional  $s$ -wave superconductor, in the presence of a uniform applied supercurrent. The supercurrent induces changes in the electronic structure for the isolated vortex as well as the vortex lattice, which agree with the recent measurements in  $2H$ -NbSe<sub>2</sub> [Maldonado *et al.*, *Phys. Rev. B* **88**, 064518 (2013)]. We find that the supercurrent polarizes the core states when the vortices are pinned. This shows that the transfer of momentum from the supercurrent to the bound states and the rigidity of the wave functions must be considered for understanding the various forces acting on collectively pinned Abrikosov vortices.

PACS numbers: 74.25.N-, 74.55.+v, 74.81.-g

The quantum states bound to magnetic vortices in type-II superconductors carry information about the fundamental properties of the superconducting state. The existence of bound states was predicted long ago,<sup>1</sup> but the direct observation in NbSe<sub>2</sub> awaited the invention of the scanning tunneling microscope (STM).<sup>2</sup> The complete mapping of the tunneling conductance in real space as a function of applied bias provided a large data set, in striking agreement with the BCS predictions for the local density of states (LDOS) of a vortex.<sup>3</sup> Since then, several groups have investigated the vortex cores by STM in NbSe<sub>2</sub>,<sup>4-6</sup> in other classical superconductors,<sup>7-11</sup> in high- $T_c$  cuprates,<sup>12</sup> and, more recently, in the pnictides.<sup>13-16</sup> While in classical superconductors, including the pnictides, these studies usually reveal vortex-core spectra in good qualitative agreement with the BCS theory, significant deviations are found in high- $T_c$  superconductors, probably due to an anomalous normal state.<sup>12</sup> The interpretation of vortex-core spectra in the cuprates remains an open question.

Recently, a measurement of the vortex electronic structure in the presence of an in-plane current flow was performed in NbSe<sub>2</sub>.<sup>17</sup> When a supercurrent is established across a vortex lattice, a “Lorentz force” acts on the vortices in the direction normal to the applied current.<sup>18</sup> In Ref. 17, the current was sufficiently small for the force to remain below the depinning threshold, and the authors could map the LDOS of static vortices with and without the applied current. The main observation of this experiment is that the application of a current transfers low-energy spectral weight from inside the cores, where the zero-bias conductance is reduced, to in between the vortices where it is enhanced, while the converse appears at the gap edges, where the spectral weight is enhanced inside the cores and depleted outside. The measurements also suggest that the current increases the size of the vortex cores. To interpret these trends, the authors assume that the applied current reduces the smallest gap on the two-band Fermi surface of NbSe<sub>2</sub>. This would affect the formation of Andreev bound states in the cores, diminishing their energy separation.

This interpretation refers to second-order changes in the modulus of the order parameter but ignores that the leading effect of the applied current is a distortion of the order-parameter *phase*. From a mesoscopic point of view, a uni-

form supercurrent in a vortex lattice can be regarded as a distortion of the phase. The modulus of the pair wave function  $\Psi(\mathbf{r}) = |\Psi(\mathbf{r})|e^{i\chi(\mathbf{r})}$  vanishes at the vortex centers and approaches the constant zero-field value at a distance  $r_c \approx \xi$  from the cores, where  $\xi$  is the superconducting coherence length. Its phase  $\chi(\mathbf{r})$  winds by  $2\pi$  around each vortex. The topological defect associated with the phase winding is responsible for the formation of the vortex bound states.<sup>19,20</sup> The supercurrent  $\mathbf{J}_\chi \approx (e\hbar/m)|\Psi|^2\nabla\chi$  (neglecting magnetic contributions) circulates around each vortex. Its intensity vanishes linearly in the cores, decreases as  $1/r$  at intermediate distances shorter than the penetration depth, and is maximum at a distance  $\sim r_c$  from the core centers. In the presence of an applied uniform superflow, the pair wave function becomes  $\Psi(\mathbf{r}) = |\Psi(\mathbf{r})|e^{i[\chi(\mathbf{r})+\mathbf{q}\cdot\mathbf{r}]}$ , where the applied current  $\mathbf{J}_q \approx (e\hbar/m)|\Psi|^2\mathbf{q}$  vanishes in the vortex cores like the vortex-lattice supercurrent. The phase distortion displaces the electronic levels by the Doppler shift effect,<sup>21</sup> and is therefore expected to change the vortex LDOS.

The effect of this phase distortion on the LDOS is studied here in a simple one-band tight-binding model in two dimensions. This is not intended to be a realistic model for NbSe<sub>2</sub>. However, the features demonstrated here are expected to be generic, and to apply to more sophisticated models as well. The tight-binding and superconducting parameters are chosen in a way that allows a semiquantitative comparison with NbSe<sub>2</sub>. In a previous study, it was shown that the vortex-core LDOS is weakly sensitive to distortions of the phase which are random but is qualitatively modified by distortions which carry a topological defect, like a nearby antivortex.<sup>20</sup> The case of a uniform distortion was not considered. In the present study, we keep the modulus of the order parameter fixed and perturb the phase in order to simulate a uniform applied current. This produces an exchange of spectral weight between the core and the outside and an apparent increase of the vortex-core size, both for an isolated vortex and for a vortex lattice. All trends observed in the NbSe<sub>2</sub> experiment<sup>17</sup> can therefore be attributed to the first-order effect of the applied current, without resorting to a reduction of the order-parameter amplitude and/or to multiband effects.

The model is a tight-binding square lattice with a dispersion  $\xi_{\mathbf{k}} = -2t[\cos(k_x a) + \cos(k_y a)] - \mu$ , and an  $s$ -wave

superconducting gap  $\Delta$ . We use  $\Delta$  as the unit of energy, the lattice parameter  $a$  as the unit of length, and we set the chemical potential to  $\mu = 2t > 0$ . This locates the van Hove singularity at the positive energy  $2t$ , and produces an electronlike Fermi surface corresponding to an electron density  $n \approx 0.4$  and a Fermi wave vector  $k_F \approx \pi/2$ . With this choice, and if  $\Delta < t$ , the normal-state DOS is approximately constant—reducing the band-structure effects to a minimum—in the energy range  $\pm 3\Delta$ , where we aim to study the effect of the applied current. The isolated vortex and the vortex-lattice structures are studied in a finite mesh of size  $M \times M$  ( $M = 71$ ). After computing the lattice Green's function,

$$G_{rr'}(\varepsilon) = G_{rr'}^0(\varepsilon) + \sum_{r_1 r_2} G_{rr_1}^0(\varepsilon) \Sigma_{r_1 r_2}(\varepsilon) G_{r_2 r'}(\varepsilon), \quad (1)$$

the relation  $N(\mathbf{r}, \varepsilon) = -(2/\pi) \text{Im} G_{rr}(\varepsilon)$  allows one to obtain the LDOS. The normal-state Green's function  $G_{rr'}^0(\varepsilon) = (1/N^2) \sum_{\mathbf{k}} e^{i\mathbf{k} \cdot (\mathbf{r} - \mathbf{r}')} / (\varepsilon - \xi_{\mathbf{k}} + i0^+)$  is calculated on a much larger  $N \times N$  mesh ( $N = 1024$ ), taking advantage of the translation invariance. The self-energy is<sup>22</sup>

$$\Sigma_{rr'}(\varepsilon) = -\Psi(\mathbf{r}) G_{r'r}^0(-\varepsilon) \Psi^*(\mathbf{r}'), \quad (2)$$

where the local  $s$ -wave order parameter  $\Psi(\mathbf{r})$  describes an isolated vortex at the central site or a vortex lattice, as well as the applied current.

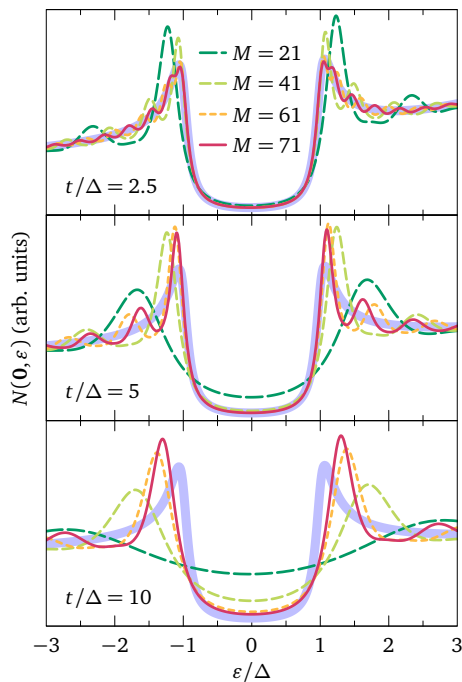


FIG. 1. Finite-size effects. The thick solid lines show the exact DOS calculated for each value of  $t$  at zero field and without applied current. The thin lines show the LDOS calculated at the central site of a  $M \times M$  mesh, setting  $\Psi(\mathbf{r}) = \Delta$  in Eq. (2). Finite-size effects are small for  $t = 2.5$  and  $M = 71$  but remain significant for the largest  $M$  if  $t = 10$ , even at subgap energies.

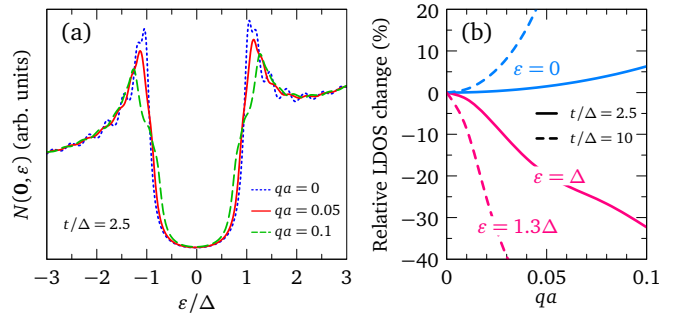


FIG. 2. (a) Zero-field LDOS at the center of the  $71 \times 71$  mesh in the absence of superflow (dotted line), and in a uniform superflow with  $q = 0.05$  (solid line) and  $q = 0.1$  (dashed line). (b) Relative variation of the LDOS at zero energy and at the gap edge versus the applied current. The solid lines are for  $t = 2.5$  ( $k_F \xi \sim 3$ ); the dashed lines are for  $t = 10$  ( $k_F \xi \sim 13$ ). Due to finite-size effects, the gap edge is at  $1.3$  for  $t = 10$ .

In the experiment,<sup>17</sup> the zero-field spectrum is considerably broadened as compared to an ideal  $s$ -wave superconducting DOS. This is not due to the finite temperature, as the latter was set to 200 mK, which is  $\sim 100$  times smaller than the NbSe<sub>2</sub> gap of  $\sim 1.3$  meV. Impurity scattering is the next candidate. We introduce a phenomenological impurity scattering through the substitution  $\varepsilon \rightarrow \varepsilon + i\Gamma$  in the definition of  $G_{rr'}^0(\varepsilon)$ . Setting  $\Gamma = 0.1$ , we obtain a zero-field spectrum in good qualitative agreement with the NbSe<sub>2</sub> spectrum. This value of  $\Gamma$  will be used throughout. Before fixing the hopping  $t$ , we need to consider finite-size effects. The latter are often overlooked in LDOS calculations for vortices, but can be significant, even on a mesh as large as  $71 \times 71$ . In our setup, the finite-size effects increase with increasing  $t$ , as shown in Fig. 1. In order to have small finite-size effects with  $M = 71$ , we must take  $t \lesssim 2.5$ . This is not far from the quantum limit  $k_F \xi = 1$ . Using the BCS relation  $k_F \xi = 2E_F / (\pi \Delta)$  and the value  $E_F = 2t$  corresponding to our dispersion, we estimate  $k_F \xi = (4/\pi)(t/\Delta) \lesssim 3$ . The typical value for NbSe<sub>2</sub> may be estimated as  $k_F \xi = m^* v_F \xi / \hbar \sim 11$ –14, using the values  $m^* = 2m$ ,  $v_F = 8.2 \times 10^6$  cm/s, and  $\xi = 79$ –100 Å reported in Ref. 3. The calculation for higher values of  $k_F \xi$  require larger  $M$ , but the calculation scales as  $M^4$ . One may however argue that the variations of the LDOS induced by the applied current are less sensitive to the boundary than the LDOS itself. Hereafter we will present results for  $t = 2.5$  and for  $t = 10$  ( $k_F \xi \sim 13$ ), focusing in the latter case, which is relevant for a comparison with NbSe<sub>2</sub>, on the LDOS variations induced by the applied current.

The value of the current flowing around the vortices below the STM tip is not known precisely.<sup>17</sup> Our approach to calibrate the current in the model is to require that its effect on the zero-field LDOS is similar to the observations made at zero field in NbSe<sub>2</sub>. We consider a uniform superflow along  $x$  at zero field by setting  $\Psi(\mathbf{r}) = \Delta e^{-iqx}$  in Eq. (2). The resulting LDOS is compared with the zero-current LDOS in Fig. 2. The applied current increases the conductance in the gap and decreases the conductance at the gap edges,

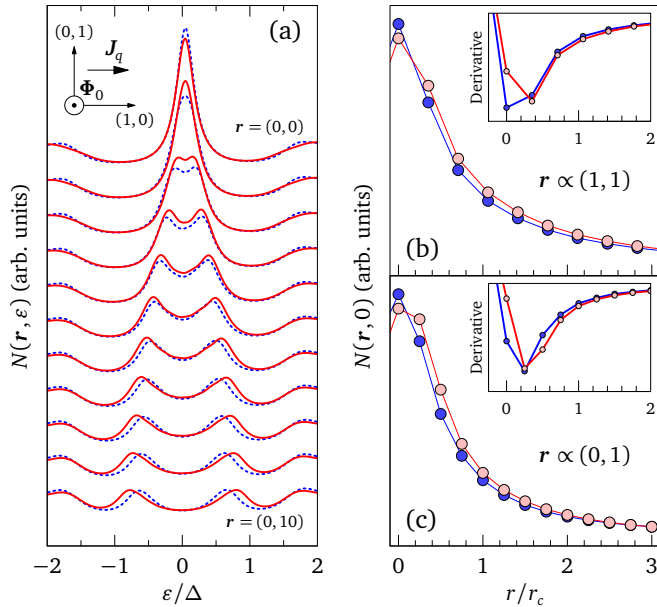


FIG. 3. (a) LDOS along the (0, 1) direction for an isolated vortex at position (0, 0) with  $t = 10$  and  $r_c = 4$ . The dotted lines are for  $q = 0$  and the solid lines for  $q = 0.02$ . The inset shows the direction of the applied current;  $\Phi_0$  is the vortex magnetic flux vector. The zero-energy LDOS along the diagonal and along the  $y$  axis are shown in (b) and (c), respectively, without (full symbols) and with (empty symbols) the applied current. The insets show  $dN(r, 0)/dr$  obtained by numerical differentiation.

consistent with the observations.<sup>17</sup> We obtain a semiquantitative agreement with the measurements performed in a current of 10.6 mA, namely, an  $\sim 20\%$  drop of the conductance at the peak energy—by setting  $q = 0.05$  for  $t = 2.5$ , and  $q = 0.02$  for  $t = 10$ . With these values, the applied current remains much smaller than the largest supercurrent circulating around vortices, as discussed below.

We now turn to the case of an isolated vortex in a uniform applied current. For the order parameter we assume the form  $\Psi(\mathbf{r}) = \Delta \tanh(r/r_c) e^{-i(\vartheta+qx)}$ , where  $\mathbf{r} = (x, y) = r(\cos\vartheta, \sin\vartheta)$ , the origin being at the center of the  $M \times M$  mesh. The vortex-core radius  $r_c$  is estimated as  $r_c \sim \xi$ , with  $k_F \xi = (4/\pi)(t/\Delta)$ , and  $k_F \approx \pi/(2a)$ . We thus obtain  $r_c/a = (2/\pi)^2(t/\Delta)$ . The ratio of the applied and vortex currents is  $J_q/J_\chi = qr$ , and the vortex current is largest at  $r = r_c$ . Therefore, if  $qr_c \ll 1$ , the applied current is much smaller than the maximum vortex-induced supercurrent. For  $t = 2.5$  and  $t = 10$ , we have  $r_c \approx 1$  and  $r_c \approx 4$ , respectively, such that the condition is satisfied with the respective values  $q = 0.05$  and  $q = 0.02$ . The model assumes that the vortex is pinned without being actually close to a pinning center. This is appropriate in a regime of collective pinning, as in the NbSe<sub>2</sub> experiments.

For  $q = 0$ , the calculated vortex LDOS shown in Fig. 3(a) exhibits the well-known structures common to BCS  $s$ -wave vortices:<sup>1,3,23–25</sup> a low-energy peak at the vortex center, which splits with increasing distance from the center. In the presence of the current, the central peak is reduced, while

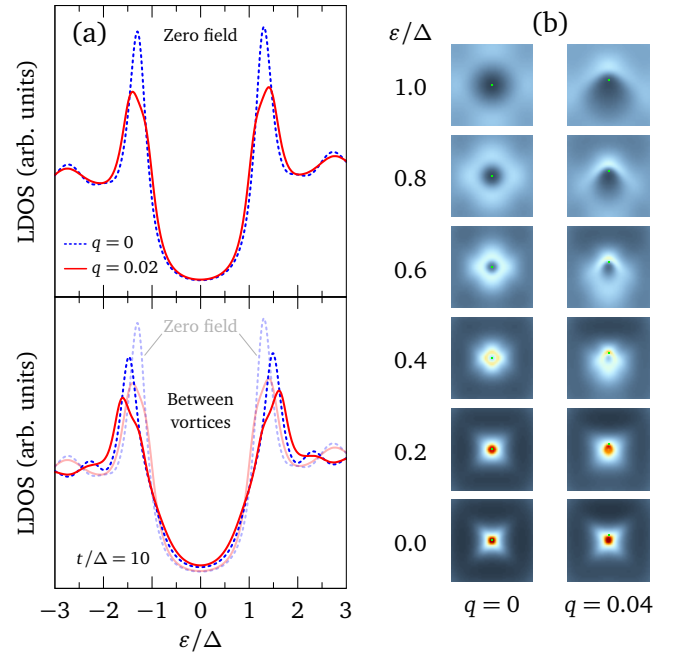


FIG. 4. (a) Zero-field LDOS at the center of the  $71 \times 71$  mesh (top panel) and LDOS in a triangular vortex lattice at equal distance from three neighboring vortices (bottom panel: the data of the top panel is repeated for comparison). The dotted lines are for  $q = 0$  and the solid lines for  $q = 0.02$ . (b) LDOS in real space for a vortex core in a vortex lattice at various energies without (left) and with (right) an applied current. The region shown is the  $51 \times 51$  central part of the  $71 \times 71$  mesh. The color scale is the same in all images. The green dot is the point where  $|\Psi(\mathbf{r})| = 0$ .

the zero-energy LDOS increases with respect to the zero-current case when moving outside the core. The trend is opposite slightly below the gap edges: the LDOS is enhanced in the core and reduced outside the core. Figures 3(b) and 3(c) compare the zero-energy LDOS and its numerical derivative, with and without the current, on the lines going from the center of the vortex along the (1, 1) and (0, 1) directions, respectively. These results show striking similarities with the experiment,<sup>17</sup> in particular, an apparent increase of the vortex-core size revealed by a displacement of the minimum in the LDOS derivative. The figure also suggests that the energy separation between the core states is reduced by the uniform current for  $r \lesssim r_c$ , and increased for  $r > r_c$ . The same behavior is observed for  $t = 2.5$ , which excludes a finite-size effect. This phenomenon is related to the polarization of the vortex-core states, as discussed further below.

If the vortex belongs to a vortex lattice, we found that the core spectra are slightly broadened with respect to those in Fig. 3 but that the general trends remain unchanged. We considered a triangular vortex lattice with a nearest-neighbor vortex distance of 50. With this value, the LDOS far from vortices differs from the zero-field LDOS, as shown in Fig. 4(a): there are more states in the gap at finite field, the peaks are reduced, and the gap appears slightly larger, in good qualitative agreement with the NbSe<sub>2</sub> data.<sup>17</sup> Fig-

ure 4(b) compares the vortex-core LDOS in a vortex lattice with and without the applied current. The current-induced expansion of the core size can be distinguished at low energy (we used here a larger current  $q = 0.04$  in order to emphasize this). Note that the LDOS has an energy-dependent fourfold anisotropy due to the underlying square symmetry of the model.<sup>26</sup> At higher magnetic fields (intervortex distance  $\lesssim 30$ ), a sixfold anisotropy develops due to the vortex lattice.

The images in Fig. 4(b) for  $q = 0.04$  show a systematic deformation in the direction  $(0, -1)$ , which is the direction of the force  $\mathbf{J}_q \times \Phi_0$  (downwards in the figures). At zero energy, the LDOS peak does not coincide with the point where  $|\Psi(\mathbf{r})| = 0$ , but is shifted by the applied current in the direction of the force. In Figs. 3 and 4(b), this has been corrected by displacing the origin in the direction  $(0, -1)$  by two and three lattice spacings, respectively, in the finite-current data. With increasing energy, the center of gravity of the vortex bound states moves further in the direction of the force. Thus the whole electronic structure of the vortex is bent by the applied current. The spatial separation between the zero of  $|\Psi(\mathbf{r})|$  and the center of the bound states is another illustration of the key role played by the order-parameter *phase* in the formation of the vortex states, and the marginal relevance of its modulus.<sup>20</sup> A displacement of the LDOS peak with respect to the phase singularity point was also found in vortex-antivortex pairs.<sup>27</sup> Because  $\Psi(\mathbf{r})$  is artificially pinned in our non-self-consistent calculations and the high-energy states must remain orthogonal to the low-lying ones, the wave functions sharpen on one side of the vortex and extend on the other side, leading to the characteristic polarization seen in Fig. 4(b). This polarization explains the shift of the core-state peaks to higher energies

in Fig. 3(a). In the direction  $(0, 1)$ , the bound states pile up more densely in real space, and the core-state peaks disperse more rapidly with distance. The opposite behavior occurs in the direction  $(0, -1)$ , where the core-state peaks are shifted to *lower* energies (not shown in the figure) with respect to the zero-current LDOS. No energy shift, but a slight deformation of the peaks, is observed in the  $x$  direction parallel to the current. Observing the polarization of the LDOS in the direction normal to the current is an interesting challenge for future STM experiments.

The origin of the force acting on vortices in the presence of a supercurrent has been discussed by many authors.<sup>19,28-32</sup> Our calculations show that the superflow transfers momentum into the bound states, resulting in a polarization of the wave functions if the vortex is pinned. On one side of the vortex, the bound states are more localized, because the applied supercurrent is contrary to the vortex supercurrent and the superfluid velocity is reduced. On the other side, the two supercurrents add up and the wave function is more extended. This effect may be considered to have a magnetic origin, the vector potential of the applied current changes the phase relation between the electron and hole parts of the Bogoliubov excitations in the vortex, but is obviously different from the electromagnetic interaction between the applied supercurrent and the magnetic flux carried by the vortex. The polarizability of the vortex-core states has not been considered so far in the study of the interaction between currents and vortices, and between different vortices. A microscopic calculation of the vortex energy in a uniform applied current would be a first step in this direction. This is not an easy task, however, because a self-consistent determination of the fields and currents is required for a precise comparison of the various forces.

- 
- <sup>1</sup> C. Caroli, P. G. de Gennes, and J. Matricon, *Phys. Lett.* **9**, 307 (1964).
  - <sup>2</sup> H. F. Hess, R. B. Robinson, R. C. Dynes, J. M. Valles, and J. V. Waszczak, *Phys. Rev. Lett.* **62**, 214 (1989).
  - <sup>3</sup> F. Gygi and M. Schlüter, *Phys. Rev. B* **41**, 822 (1990); *Phys. Rev. B* **43**, 7609 (1991).
  - <sup>4</sup> C. Renner, A. D. Kent, P. Niedermann, Ø. Fischer, and F. Lévy, *Phys. Rev. Lett.* **67**, 1650 (1991).
  - <sup>5</sup> S. Behler, S. H. Pan, P. Jess, A. Baratoff, H.-J. Güntherodt, F. Lévy, G. Wirth, and J. Wiesner, *Phys. Rev. Lett.* **72**, 1750 (1994).
  - <sup>6</sup> A. M. Troyanovski, J. Aarts, and P. H. Kes, *Nature (London)* **19**, 665 (1999).
  - <sup>7</sup> Y. DeWilde, M. Iavarone, U. Welp, V. Metlushko, A. E. Koshelev, I. Aranson, G. W. Crabtree, and P. C. Canfield, *Phys. Rev. Lett.* **78**, 4273 (1997).
  - <sup>8</sup> H. Sakata, M. Oosawa, K. Matsuba, N. Nishida, H. Takeya, and K. Hirata, *Phys. Rev. Lett.* **84**, 1583 (2000).
  - <sup>9</sup> M. R. Eskildsen, M. Kugler, S. Tanaka, J. Jun, S. M. Kazakov, J. Karpinski, and Ø. Fischer, *Phys. Rev. Lett.* **89**, 187003 (2002).
  - <sup>10</sup> C. E. Sosolik, J. A. Stroscio, M. D. Stiles, E. W. Hudson, S. R. Blankenship, A. P. Fein, and R. J. Celotta, *Phys. Rev. B* **68**, 140503 (2003).
  - <sup>11</sup> I. Guillamón, H. Suderow, S. Vieira, L. Cario, P. Diener, and P. Rodière, *Phys. Rev. Lett.* **101**, 166407 (2008).
  - <sup>12</sup> See, e.g., Ø. Fischer, M. Kugler, I. Maggio-Aprile, C. Berthod, and C. Renner, *Rev. Mod. Phys.* **79**, 353 (2007), and references therein.
  - <sup>13</sup> Y. Yin, M. Zech, T. L. Williams, X. F. Wang, G. Wu, X. H. Chen, and J. E. Hoffman, *Phys. Rev. Lett.* **102**, 097002 (2009).
  - <sup>14</sup> L. Shan, Y.-L. Wang, B. Shen, B. Zeng, Y. Huang, A. Li, D. Wang, H. Yang, C. Ren, Q.-H. Wang, S. H. Pan, and H.-H. Wen, *Nat. Phys.* **7**, 325 (2011).
  - <sup>15</sup> C.-L. Song, Y.-L. Wang, P. Cheng, Y.-P. Jiang, W. Li, T. Zhang, Z. Li, K. He, L. Wang, J.-F. Jia, H.-H. Hung, C. Wu, X. Ma, X. Chen, and Q.-K. Xue, *Science* **332**, 1410 (2011).
  - <sup>16</sup> T. Hanaguri, K. Kitagawa, K. Matsubayashi, Y. Mazaki, Y. Uwatoko, and H. Takagi, *Phys. Rev. B* **85**, 214505 (2012).
  - <sup>17</sup> A. Maldonado, S. Vieira, and H. Suderow, *Phys. Rev. B* **88**, 064518 (2013).
  - <sup>18</sup> P. G. de Gennes, *Superconductivity of Metals and Alloys*, Advanced Book Classics (Perseus, Cambridge, 1999).
  - <sup>19</sup> G. E. Volovik, *JETP Lett.* **57**, 244 (1993).
  - <sup>20</sup> C. Berthod, *Phys. Rev. B* **71**, 134513 (2005).
  - <sup>21</sup> G. E. Volovik, *JETP Lett.* **58**, 469 (1993).
  - <sup>22</sup> L. P. Gorkov, *Sov. Phys. JETP* **7**, 505 (1958).
  - <sup>23</sup> J. Bardeen, R. Kümmel, A. E. Jacobs, and L. Tewordt, *Phys. Rev.*

- [187, 556 \(1969\)](#).
- <sup>24</sup> J. D. Shore, M. Huang, A. T. Dorsey, and J. P. Sethna, [Phys. Rev. Lett. \*\*62\*\*, 3089 \(1989\)](#).
- <sup>25</sup> N. Hayashi, T. Isoshima, M. Ichioka, and K. Machida, [Phys. Rev. Lett. \*\*80\*\*, 2921 \(1998\)](#).
- <sup>26</sup> Y.-D. Zhu, F. C. Zhang, and M. Sigrist, [Phys. Rev. B \*\*51\*\*, 1105 \(1995\)](#).
- <sup>27</sup> A. S. Mel'nikov, D. A. Ryzhov, and M. A. Silaev, [Phys. Rev. B \*\*79\*\*, 134521 \(2009\)](#).
- <sup>28</sup> N. B. Kopnin and V. E. Kravtsov, [Sov. Phys. JETP \*\*44\*\*, 861 \(1976\)](#).
- <sup>29</sup> M. Stone, [Phys. Rev. B \*\*54\*\*, 13222 \(1996\)](#).
- <sup>30</sup> D.-X. Chen, J. J. Moreno, A. Hernando, A. Sanchez, and B.-Z. Li, [Phys. Rev. B \*\*57\*\*, 5059 \(1998\)](#).
- <sup>31</sup> O. Narayan, [J. Phys. A: Math. Gen. \*\*36\*\*, L373 \(2003\)](#).
- <sup>32</sup> A. S. Mel'nikov and A. V. Samokhvalov, [JETP Lett. \*\*94\*\*, 759 \(2011\)](#).